Journal of Micromechanics and Microengineering

High density cleanroom-free microneedle arrays for pain-free drug delivery

OPEN ACCESS
IOP Publishing
Journal of Micromechanics and Microengineering
J. Micromech. Microeng. **33** (2023) 015005 (8pp)
https://doi.org/10.1088/1361-6439/aca4da

High density cleanroom-free microneedle arrays for pain-free drug delivery

Thomas Lijnse[1,*], Kazim Haider[1], Catherine Betancourt Lee[1] and Colin Dalton[1,2]

[1] Department of Biomedical Engineering, University of Calgary, Calgary, Canada
[2] Department of Electrical and Software Engineering, University of Calgary, Calgary, Canada

E-mail: thomas.lijnse@ucalgary.ca

Received 26 August 2022, revised 13 October 2022
Accepted for publication 22 November 2022
Published 5 December 2022

Abstract

The purpose of this work is to demonstrate the fabrication process for cleanroom-free solid metal microneedles and perform quantification of insertion profiles. Metal microneedles were created using a modified wirebonding process and inserted into porcine tissue to determine design efficacy. Microneedle arrays were analyzed through optical imaging and scanning electron microscopy. Insertion forces were measured using combined uniaxial load cell and resistance measurement data. Microneedle arrays were successfully inserted into porcine tissue with high repeatability and reliability. These arrays demonstrate lower or equivalent insertion forces (less than 3 N) to other forms of microneedles in the literature without the need for complex cleanroom fabrication processes. The microneedle fabrication method presented here rapidly produces mass manufacturable, high-quality microneedle arrays with minimal insertion forces, able to reliably penetrate tissue samples. The manufacturing method presented here achieved array densities as high as 3200 needles cm^{-2}. These microneedle arrays demonstrate simple fabrication of a reliable, high-density, pain-free drug delivery system, with potential applications in biosensing and electric field modulated drug delivery.

Supplementary material for this article is available online

Keywords: transdermal drug delivery, microfabrication, microneedles, wirebonding

(Some figures may appear in color only in the online journal)

1. Introduction

Nearly 16 billion hypodermic injections are administered worldwide annually [1]. Needles are one of the most ubiquitous medical tools, yet approximately one in ten Americans suffer from needle-phobia and will actively avoid or refuse medical care in order to prevent the pain and discomfort associated with hypodermic injections [2]. Medical care avoidance causes significant long-term health complications and increases burden on already overloaded healthcare systems. Microneedles are sub-millimeter structures capable of delivering drugs and interacting with sub-dermal tissues with minimal pain or discomfort [3, 4]. Due to the lack of direct interaction with nervous tissues, there is significantly reduced pain during injection, however there is still experienced patient pain and discomfort due to the localized pressure required to insert microneedle arrays. This experienced pain can be directly correlated to the peak forces occurring during microneedle insertion [5]. In order to optimize microneedle

* Author to whom any correspondence should be addressed.

arrays for pain free drug delivery, insertion forces must be minimized while maintaining a mechanically robust needle to penetrate the outer layers of the skin without fracture or bending.

1.1. Microneedles for transdermal drug delivery

Skin is the body's first line of defense for all organic dangers, serving as an anti-bacterial, high impedance, ultraviolet protective, and temperature resistant barrier to our immune systems. Most of this protection comes from the outer layer of the skin, called the *stratum corneum* (SC), which is a densely packed layer of corneocytes and connective tissue approximately 20 mm thick, with some variation depending on location [6, 7]. In order to transdermally deliver pharmaceuticals or interact with cardiac or bioelectric systems the SC must be pierced, as it will block all compounds less than 500 Da [8]. In order to deliver drugs, microneedles pierce the SC but are smaller in height than 1 mm, in order to avoid damage or interaction with nervous tissues in the lower dermis, which are typically 1.5 mm in depth. Microneedles are also gaining popularity as an interfacing method for biosensors [9, 10]. There are three distinct forms of microneedles, solid, hollow, and dissolvable, each with strengths and weaknesses.

Hollow microneedles are miniaturized hypodermic needles with a hollow central channel for fluid delivery or extraction. While an incredibly effective form of microneedle [11], fabrication is typically highly complex [12, 13], and due the scale of features, are prone to fracture, insertion failure, and channel clogging. Dissolvable microneedles are made of a bioresorbable material with suspended pharmaceutical compounds. As the microneedles are inserted, they degrade and deliver highly targeted therapy. These dissolvable needles do not have issues with channel clogging and are generally less prone to fracture or mechanical failure. In addition, if fractured needle tips or detritus is left behind in the body, it will be resorbed rather than potentially causing granulomas or other lasting tissue injury [14]. The major fallback of dissolvable needles is that they face similar microfabrication challenges and typically the materials used do not have mechanical properties suited to effective tissue insertion [15].

Solid microneedles are an adaptable form of microneedle that can be fabricated relatively easily compared to hollow and dissolvable needles [16]. These needles can either be used as skin pre-treatment to increase or allow uptake of topical compounds, or can be coated similarly to dissolvable needles, but with better overall mechanical properties [3]. Solid microneedles can generally be built with sharper tips (smaller tip radius), smaller dimensions (length, diameter), and improved mechanical parameters, but broadly suffer from limited drug delivery capabilities. Even with the advantages above, most solid microneedles still require cleanroom fabrication facilities. There has been limited work in the development of cleanroom-free microneedle arrays, but they do not reach the same low insertion forces or reliability of cleanroom fabricated arrays, and require either time-intensive or chemical heavy fabrication processes [17, 18].

Metal microneedles or otherwise conductive microneedles, are also being investigated for their applications in direct biosensing, whether bioelectric [19–21] or biochemical [10, 22]. Presently microneedles made for these purposes are either large form factor, resulting in high tissue damage and insertion forces, or require complex coating processes after production. Here we present a novel method of solid metal microneedle fabrication that is high-speed, reliable, and cleanroom-free using biocompatible materials suited to drug delivery and integrated biosensing.

2. Methods

2.1. Fabrication

Microneedle fabrication was performed using automated (F&S Bondtec, 56XXi) or semi-automated (TPT HB16) wirebonders adjusting a previously reported process by our group [23]. A ball bonding process has been adjusted, as seen in figure 1, to extrude a specific length of wire without causing undue stress at the initial ball bond. Figure 1 shows individual stills of the production process, and an animation of the process is available in the supplementary materials. When performing the second bond, the applied force and ultrasonic power have been increased, while the overall bond time has been decreased, leading to an unsuccessful bond that causes a weak point in the wire. When the bond head is retracted, the wire snaps at the weak point, leaving a chisel-tip shaped needle standing straight up. A close-up view of this tip shape can be seen in figure 2. This beveled tip shape is similar to existing hypodermic needle tip geometries, and reduces overall insertion trauma and required insertion forces. Figure 2(b) shows that the fabrication process, relying on the natural ductility of gold, produces an extremely sharp cutting surface.

Using the automated equipment, this process is fully controllable and adjustable. The bond head can be retracted directly above the first bond, leaving a wire that stands directly vertical. Using the semi-automated bonder, the bond head retracts above the second bond, leaving the microneedles at a significant angle (30° from vertical). This means that in figure 1(b), the bond head would retract straight up instead of returning above the original bond. In this case the bond head is manually lowered and the individual needles are pushed into an upright position. The impacts of the limitations of the semi-automated wirebonder can be seen in the slight bends of the wire in figure 2(a), showing irregularities in the fabrication process. While these bends can be quite severe, the surface of the skin is incredibly non-uniform and a perfect axial load cannot be expected, so the varying angles of the tips may not be problematic during insertion. Additionally, there are grid non-uniformities due to manual placement of the needles using an optical guide. Needle densities and heights are calculated using a calibrated microscope. The semi-automated equipment used here is capable of producing microneedles at a rate of approximately 1 needle 45 s^{-1},

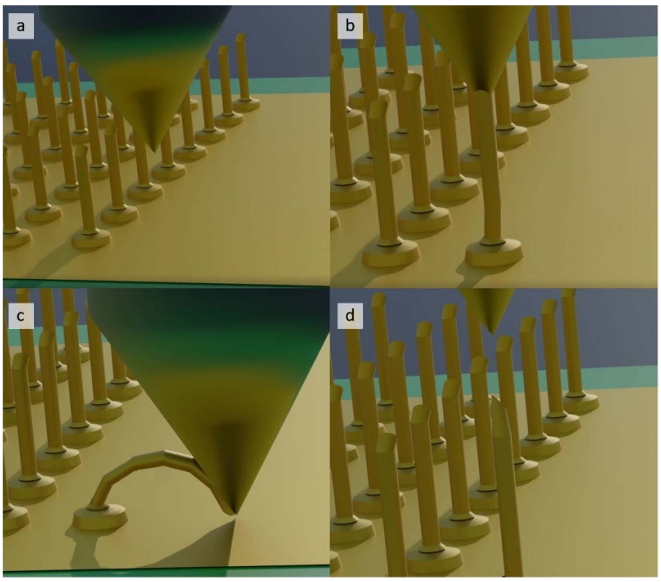

Figure 1. Images detailing the microneedle fabrication process. (a) Bond head approaches substrates with microneedles already previously fabricated. (b) Ball bond is created and wire is extruded. (c) Wire is impinged against substrate to weaken at a set point. (d) Bond head is returned above the original ball bond and is retracted with wire clamped to break the wire at set point.

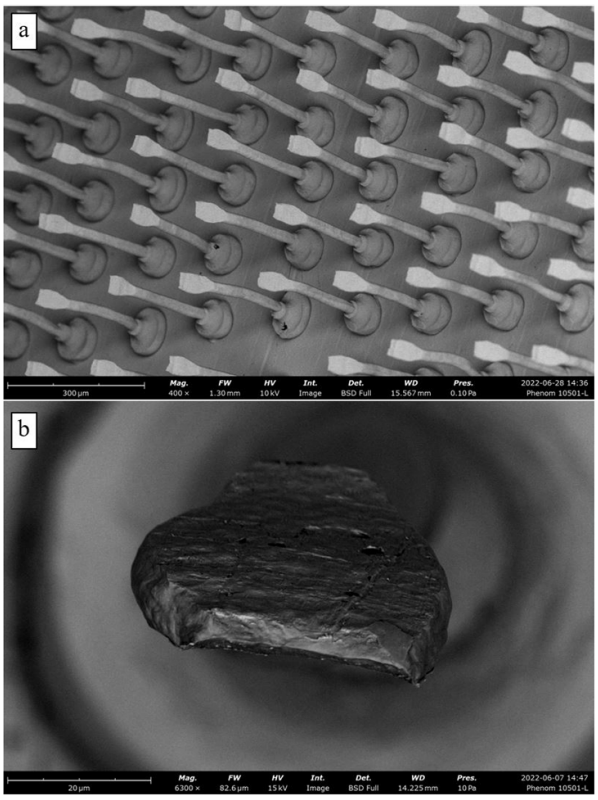

Figure 2. SEM images of fabricated microneedles. Top: high-density microneedle array with ∼3100 needles cm^{-2}. Scale bar is 300 μm. Bottom: direct view of 'chisel-tip' of microneedles. Needle deflection angle can be seen in the background. Scale bar is 20 μm.

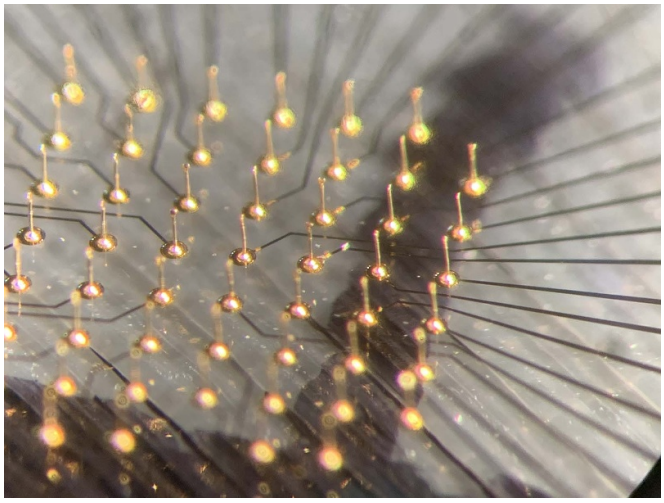

Figure 3. Representative array showing individually addressable electrodes with microneedles fabricated using a fully automatic wirebonder. Electrodes shown here are fabricated on a glass substrate.

while the fully automated equipment is capable of up to 1 needle s^{-1}.

Microneedle arrays were fabricated on two forms of substrate. Printed circuit board (PCB) substrates produced using electroless nickel electroless palladium immersion gold (ENEPIG) acquired from PCBWay were used as bulk surface substrates. Thicknesses of these ENEPIG boards were 200 μin nickel, 2 μin palladium, and 2 μin gold (specifications for this are provided by the manufacturer within the bounds of IPC-4556). ENEPIG is a preferred bonding target for gold ball bonding [24], and is already a industry standard commercial level production process. Further, glass substrates with individually addressable electrodes were created using standard photolithographic techniques, with a 300 nm titanium layer and 700 nm gold layer. An example of this substrate can be seen in figure 3. While this photolithography is a cleanroom process, this was used a proof of principle. PCB manufacturing can accomplish cleanroom-free substrates with individually addressable bonding pads. Bonding pads for the microneedles were circles 100 mm in diameter with a pitch of 300 mm.

These microneedle arrays are capable of production on any substrate suitable for wirebonding. ENEPIG is used here due to its high reliability in the wirebonding process [24]. Further testing will explore production changes and challenges on cheaper substrates including electroplated polymers, electroless nickel immersion gold (ENIG) PCBs, and alternative substrates such as FlexPCBs. Furthermore, wire material is not limited to gold. There are several wirebonding suitable materials such as copper, aluminum, and platinum, some with lower costs. However gold is used due to its biocompatibility and, in this case, availability on wirebonding systems. The small amount of gold wire used (25 μm diameter wire, approximately 30–80 mm per array, depending on density and height), means that this is a very cost effective fabrication strategy. We estimate the average cost per array to be $0.50 USD in gold wire, and this cost will decrease with larger scale production.

2.2. Tissue insertion

In order to assess efficacy of microneedles, insertion force was measured using abdominal porcine skin samples acquired from the University of Calgary Faculty of Veterinary Medicine. Tissue samples were stored in a −4 °C freezer until required. The freeze-thaw process is known to change mechanical properties of tissue, however previous work has shown that pre-freezing and thawing of porcine skin can cause stiffening of the SC leading to a more similar mechanical model to human tissue, compared to fresh porcine tissue, and a superior model compared to frozen human tissue [25]. Furthermore, frozen porcine skin is much easier to acquire and handle. Tissue is allowed to rest at room temperature for 2 h prior to sectioning, at which point they are kept in an incubation chamber at 37 °C and high humidity to maintain approximate *in vivo* conditions prior to insertion testing. Force data collection was completed using a uniaxial load machine (Tinius Olsen H1KT) set to perform compression as seen in figure 4. A multimeter (Agilent 34461A) was connected to a computer using Keysight BenchVue software to collect resistance data during insertion. Most microneedle studies utilize similar methods for acquiring force data, however there are no standards for tissue conditions and insertion procedures, so there will be significant variation between studies depending on whether polymer films [26], porcine skin [13], human cadaver skin [27, 28], or mouse models [29] are used. This makes direct comparisons between studies difficult, however there is relative similarity between expected forces and all these works show similar insertion profiles.

In these tests, the porcine tissue is let to rest, without being fixed, on the base metal plate. The purpose of this is to allow for flexibility and natural movement of the tissue under compression conditions, such as those experienced during hypodermic injections. Fixating the tissue or otherwise placing the surface of the skin in tension would impact the overall insertion force due to the changes in tissue mechanics. Changes in insertion forces depending on fixation method are not explored in this work.

Insertion of the needles is performed at a rate of 50 μm s^{-1} to a maximum force of 30 N to ensure that all relevant data is captured. During the insertion of needles, the skin will become pretensioned due to impingement of the needle tip on the flexible surface, until the tip is able to break through the SC and penetrate further into the dermis. Due to this, a characteristic curve can be identified during needle insertion as seen in figure 5(a), where the distinct drop in experienced forces represent the peak insertion force required to penetrate the skin. As can be seen in figure 5(b), microneedle arrays can make identification of this insertion force difficult, due to overall lower insertion forces and irregularities in the skin. The surface of skin is relatively non-uniform so various needles, particularly with differences in height, will be impacting the skin at different times, which can obscure the force curve we are looking for due to overlapping insertion forces. As has been shown previously, the SC has significantly higher impedance than the dermis, and as such resistance can be measured during insertion to highlight the exact moment that the microneedles pierce through the SC [30, 31]. The exact resistance is dependent on interfacial surface area and metal conductivity, but with these microneedles we observed resistances approximately 1–50 MΩ prior to penetration and 40–200 kΩ after insertion.

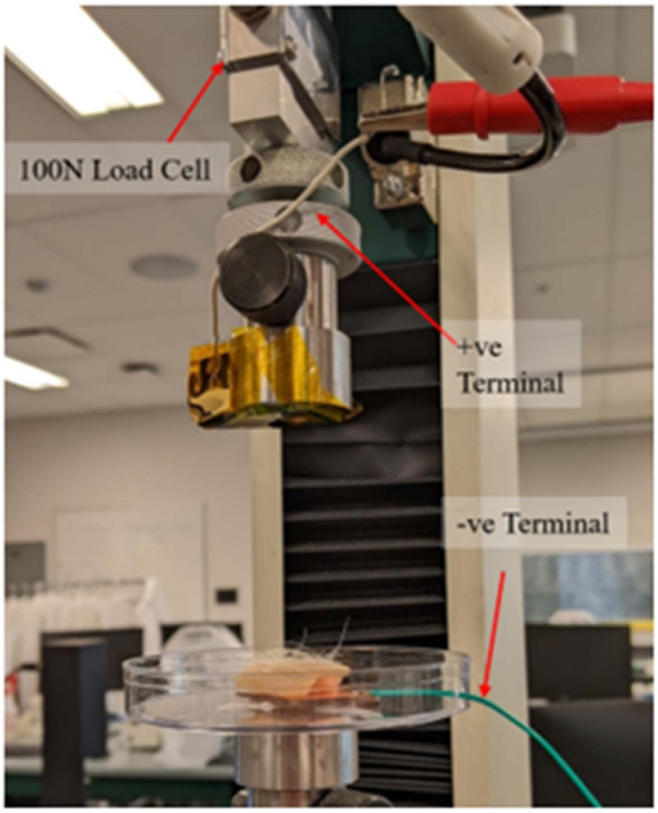

Figure 4. Image showing experimental configuration. Porcine skin is placed on top of a copper plate in a petri dish connected to the ground electrode. The microneedle arrays are connected to the top of the load cell using double-sided tape. Arrays are masked off such that only the microneedles are conductive using Kapton tape, which also secures the connection point (gold-coated polyimide sheet) for the signal line.

3. Results

To assess the insertion forces, the collected resistance data and force data were synchronized. As the force acquisition and resistance systems are not linked together, this process was performed manually. The initial decrease in resistance, shown in figure 5(b), as compression occurs is taken as time zero. Due to the manual alignment of data, there are potential small discrepancies in outcome data. This has a relatively small impact on the estimated insertion forces due to the low speed of the compression, but does likely increase the margins of error. Future analyses will sync these systems to increase overall accuracy. With force data overlaid, the moment of needle insertion can be quantified by selecting a 'threshold resistance' at which we are confident the needles

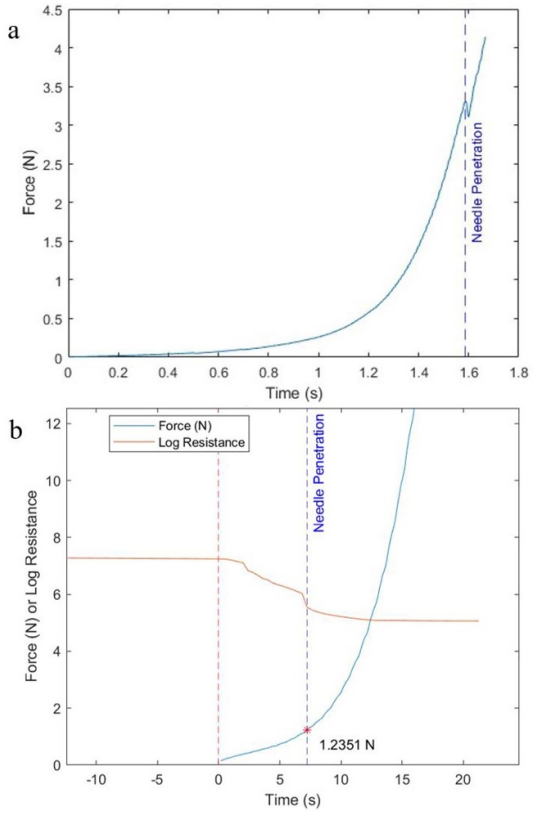

Figure 5. Images of collected force and resistance data highlighting the mechanical differences observed when using different insertion methods. (a) Insertion profile of a 23G needle into porcine skin. Peak insertion force is observed at the point before a dip in force, at 3.28 N. The travel distance (not shown) of 4.971 mm is indicative of how much the tissue compresses prior applied forces overcoming the required insertion force. (b) Insertion force profile of a microneedle array. There is no visible insertion force peak at the moment of skin penetration determined by resistance analysis. Here the force at insertion is highlighted by the red star.

have passed through the SC. Figure 6 shows the difference in force and resistance curves on a successful microneedle array insertion and a failed insertion. In this case, the threshold resistance was selected as 750 kΩ, as this was identified as a midpoint between known conductivity without SC and tissue compression with SC barrier. As can be seen in figures 6(a) and (c), the force curves are nearly indistinct and without resistance data, insertion force would be nearly impossible to quantify. Table 1 shows the insertion forces and array density for each array tested. As can be seen in figure 6(d), most needles remain standing after insertion, while some do buckle, likely due to variation in the surface skin causing non-uniform forces applied. Insertion tests performed using single microneedles and small arrays (3×3) did not result in a significant impedance drop. This implies that in tests where impedance drops were significant, a large number of microneedles were inserted. Shearing of needles did not occur during insertion, as the bond strength is higher than the lateral or pulling force applied by the tissues. Currently, insertion reliability can only be performed by manual inspection post-insertion using optical microscopy, however future efforts will investigate the use of optical tissue clearing or the use of polymeric skin models [32] to further identify insertion success rates and reliability.

Insertion forces were measured at 1.48 ± 0.77 N for PCB substrate arrays (excluding outlier P1 as indicated in table 1), and 2.91 ± 0.9 N for glass substrate arrays. The two forms of substrate do not significantly vary within the collected data ($p = 0.443$). Overall insertion forces for all substrates is 2.05 ± 1.08 N. These insertion forces are for large arrays, and are comparable in magnitude to prior studies of individual microneedles or small arrays [27, 33], and significantly lower than other bulk arrays [26]. As mentioned in section 3, direct comparisons are difficult; however, the low forces experienced by these arrays are promising for the overall efficacy of this form of microneedle.

Initial trials with needles at a height of 415 μm failed due to mechanical instability. Shortening these needles to 305 μm, as used in this work, resulted in a significant increase in array stability and insertion reliability. All microneedles used in the biological tests described here were 305 μm in length and fabricated using the same production parameters. However mechanical details between the two processes are described and there is some variability in the production process. The needles of 415 μm length had a standard deviation of 16.1 μm, while the needles of length 305 μm had a standard deviation of 15.2 μm. The standard deviation in microneedle heights is consistent across different height fabrication settings. The angle

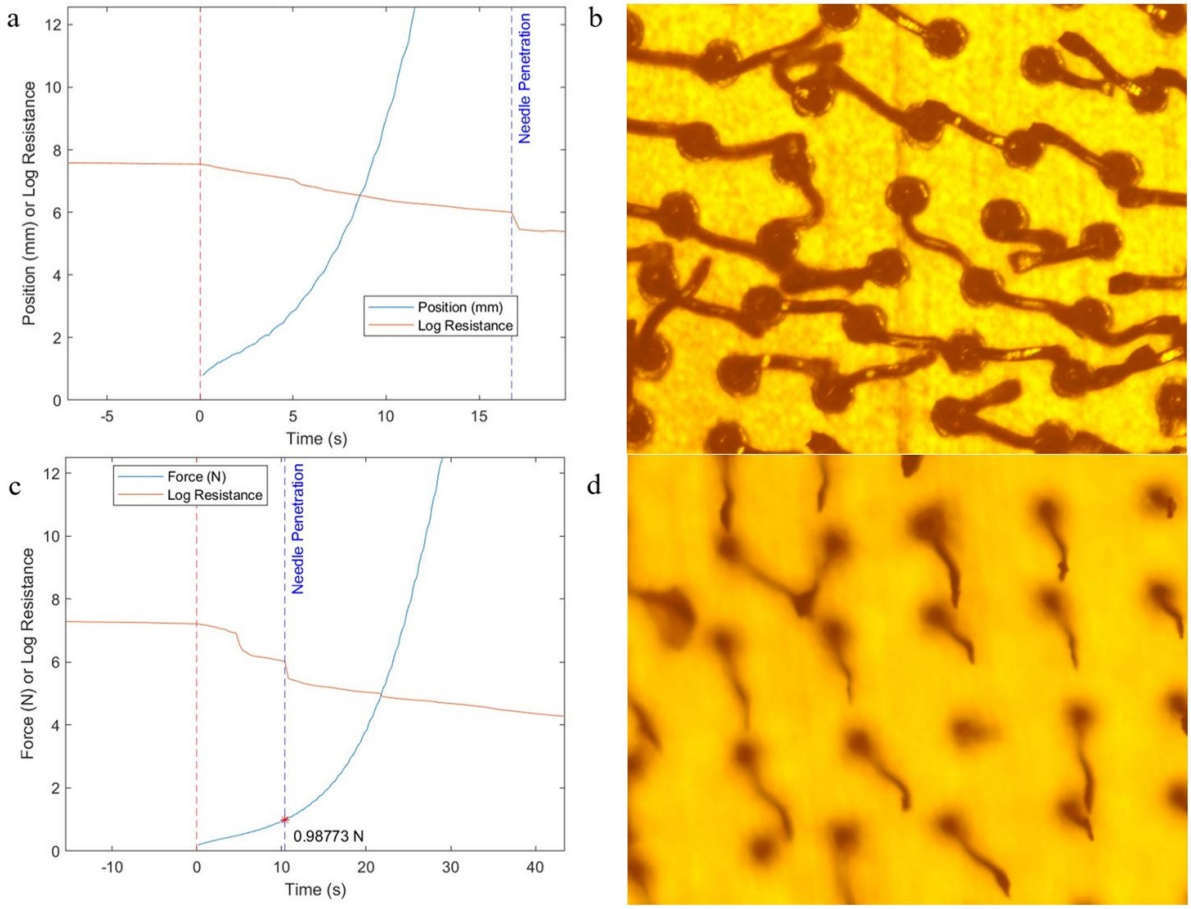

Figure 6. Images of collected force and resistance data for two separate array insertions. (a) Insertion profiles for a microneedle array with approximately 3200 needles cm^{-2}. Resistance drop indicative of tissue penetration occurs well beyond potential buckling forces for needles. (b) Post-insertion optical imaging of microneedle array used in (a). Note that all needles are buckled. (c) Insertion profiles for a microneedle array with approximately 1730 needles cm^{-2}. Resistance drop happens at expected force and compression distance. (d) Post-insertion optical imaging of microneedle array used in (c). Note that needles are still upright after insertion (tip of needle outside of substrate focus plane), indicating that buckling did not occur.

of the microneedles was assessed by taking the angle between the substrate and a line going from the center of the ball bond through the tip of the needle. The longer needles (415 μm) had an angle of 85.4° $\pm$ 4.1°, while the shorter needles (305 μm) had an angle of 88.1° $\pm$ 6.1°. These tests were not significantly different ($p = 0.16$), and the angle in the system may change with height, but it is not significantly distinct from inherent variance in the production process.

One major insertion failure occurred, as seen in figure 6(b), in which all needles buckled under insertion loads. The array which failed had an estimated density of 3100 needles cm^{-2}, which was the highest achievable density using the semi-automated bonder. This may have caused bulk failure due to the reported 'bed of nails' effect, by which high density arrays will experience overall higher loads and suffer from reduced insertion depths [34]. These microneedle arrays are expected to be single use, however several arrays were inserted multiple times until failure. While several arrays failed on second insertion, three arrays were able to be inserted at least twice, with one array being able to be inserted three times before failing. This demonstrates that these arrays have relatively strong mechanical properties and insertion reliability, which will only be increased with further process optimization and development.

Table 1. Array density and estimated insertion force.

Array	Estimated insertion force (N)	Density (needles cm^{-2})
P1[a]	5.8892	1889
P2	1.2351	855
P3	0.55646	1666
P4	1.8868	844
P5	0.98773	1729
P6	1.244	2272
P7	2.9653	2196
G1	3.12	1111
G2	3.4178	1111
G3	3.7131	1111
G4	1.3981	1111

[a] P1 was performed at a higher insertion speed than all other arrays which made identifying the exact insertion moment more difficult. This data point is included as a potential outlier.
'P' prefix indicates a PCB substrate, 'G' prefix indicates a glass substrate.

4. Discussion

There is significant need and desire for pain free drug delivery alternatives, and microneedles are a promising candidate. Here we have presented a method of producing high density microneedle arrays, customizable in height and layout depending on target application and patient. Using a modified wirebonding process we have created microneedle arrays with significantly lower insertion forces compared to literature, that are robust enough to be inserted into tissue without risk of fracture or buckling. These gold microneedles have been shown to be implementable as bulk arrays for applications in drug delivery or can be manufactured as individually electrically addressable needles with applications in biosensing. While the relationship between microneedle height and density on drug delivery is complex and reliant on needle geometry, and delivery mechanics, previous work has shown that densities in the range of several 1000 needles per square centimeter are capable of regularly and reliably delivering drug dosages [35]. With varying density and height there are tradeoffs between delivery dosage and experienced pain and tissue damage [5, 36]. The interactions between this microneedle design and optimal density and surface area are something that must be further investigated. At enhanced production rates of 1 needle s^{-1}, this method can create high density arrays at a relatively high speed in a low complexity environment, capable of larger scale automation.

With no statistical difference between substrate composition, these microneedle arrays can be fabricated on a wide variety of platforms designed for different purposes, including solid state *in vitro* systems, through to semi-flexible or flexible substrates for potential applications in wearables or biosensing. While not fully characterized in this work, the height of these needles is adjustable by varying the loop parameters used in the wirebonding process. As indicated, the longer needles fabricated for this work were mostly unsuccessful during testing, likely due to the higher susceptibility to buckling. Further testing is required to determine optimal length for maximal tissue penetration and minimized mechanical instability. Customizable array shape and localized array connectivity also allows for investigations into targeted iontophoretic or electroosmotic applications for enhanced drug delivery.

Future work will explore the pharmacokinetics of compound delivery and various delivery methods, as well as exact mechanical optimization of height, thicknesses, and density. This work demonstrates a novel cleanroom-free, low cost, reliable and mass manufacturable microneedle production method which can significantly impact microneedle research and eventually aid in the elimination of needle pain and needlephobia.

Data availability statement

All data that support the findings of this study are included within the article (and any supplementary files).

Acknowledgments

This work is supported through funding by the Natural Sciences and Engineering Research Council of Canada (NSERC), Canadian Fund for Infrastructure (CFI), Alberta Innovates (AI), and Alberta Economic Development and Trade. Further funding and support is offered by CMC Microsystems.

Furthermore, the authors would like to acknowledge the assistance of the University of Calgary Microsystems Hub and University of Alberta NanoFAB for their assistance in the array production process. The authors would also like to acknowledge F&S Bondtec (TEC Associates Inc.) for their assistance in validating the manufacturability of these microneedle arrays on automated wirebonding equipment.

Ethical Statement

The porcine tissues used in this work were obtained under the University of Calgary's Veterinary Sciences Animal Care Committee, protocol AC21-0149 VetMed320 in accordance with their regulations and they were provided to our group as secondary use, which has been authorized in the protocol by the principal investigator, Dr Robert McCorkell.

ORCID iDs

Thomas Lijnse https://orcid.org/0000-0003-4049-5215
Colin Dalton https://orcid.org/0000-0001-7855-2727

References

[1] World Health Organization Health-care waste (available at: www.who.int/news-room/fact-sheets/detail/health-care-waste) (Accessed 6 July 2022)
[2] McMurtry C M, Pillai Riddell R, Taddio A, Racine N, Asmundson G J G, Noel M, Chambers C T and Shah V 2015 Far from 'just a poke': common painful needle procedures and the development of needle fear *Clin. J. Pain* **31** S3–S11
[3] Donnelly R F, Singh T R R, Larrañeta E and McCrudden M T C (eds) 2018 *Microneedles for Drug and Vaccine Delivery and Patient Monitoring* 1st edn (New York: Wiley)
[4] Nagarkar R, Singh M, Nguyen H X and Jonnalagadda S 2020 A review of recent advances in microneedle technology for transdermal drug delivery *J. Drug Deliv. Sci. Technol.* **59** 101923
[5] Gill H S, Denson D D, Burris B A and Prausnitz M R 2008 Effect of microneedle design on pain in human subjects *Clin. J. Pain* **24** 585–94
[6] Murphrey M B, Miao J H and Zito P M 2022 Histology, Stratum Corneum *StatPearls* (Treasure Island, FL: StatPearls Publishing) (available at: www.ncbi.nlm.nih.gov/books/NBK513299/) (Accessed 6 Jul 2022)
[7] Böhling A, Bielfeldt S, Himmelmann A, Keskin M and Wilhelm K-P 2014 Comparison of the stratum corneum thickness measured *in vivo* with confocal Raman spectroscopy and confocal reflectance microscopy *Skin Res. Technol.* **20** 50–57

[8] Bos J D and Meinardi M M 2000 The 500 Dalton rule for the skin penetration of chemical compounds and drugs *Exp. Dermatol.* **9** 165–9
[9] Huang Y *et al* 2022 Implantable electronic medicine enabled by bioresorbable microneedles for wireless electrotherapy and drug delivery *Nano Lett.* **22** 5944–53
[10] Takeuchi K and Kim B 2018 Functionalized microneedles for continuous glucose monitoring *Nano Converg.* **5** 28
[11] Gupta J, Felner E I and Prausnitz M R 2009 Minimally invasive insulin delivery in subjects with type 1 diabetes using hollow microneedles *Diabetes Technol. Ther.* **11** 329–37
[12] Cárcamo-Martínez Á, Mallon B, Domínguez-Robles J, Vora L K, Anjani Q K and Donnelly R F 2021 Hollow microneedles: a perspective in biomedical applications *Int. J. Pharm.* **599** 120455
[13] Li Y, Zhang H, Yang R, Laffitte Y, Schmill U, Hu W, Kaddoura M, Blondeel E J M and Cui B 2019 Fabrication of sharp silicon hollow microneedles by deep-reactive ion etching towards minimally invasive diagnostics *Microsyst. Nanoeng.* **5** 41
[14] Rad Z F, Prewett P D and Davies G J 2021 An overview of microneedle applications, materials, and fabrication methods *Beilstein J. Nanotechnol.* **12** 1034–46
[15] Ita K 2017 Dissolving microneedles for transdermal drug delivery: advances and challenges *Biomed. Pharmacotherapy* **93** 1116–27
[16] Kim Y-C, Park J-H and Prausnitz M R 2012 Microneedles for drug and vaccine delivery *Adv. Drug Deliv. Rev.* **64** 1547–68
[17] Dabbagh S R, Sarabi M R, Rahbarghazi R, Sokullu E, Yetisen A K and Tasoglu S 2021 3D-printed microneedles in biomedical applications *iScience* **24** 102012
[18] Nejad H R, Sadeqi A, Kiaee G and Sonkusale S 2018 Low-cost and cleanroom-free fabrication of microneedles *Microsyst. Nanoeng.* **4** 1–7
[19] Debener S, Emkes R, De Vos M and Bleichner M 2015 Unobtrusive ambulatory EEG using a smartphone and flexible printed electrodes around the ear *Sci. Rep.* **5** 16743
[20] Wang R, Jiang X, Wang W and Li Z 2017 A microneedle electrode array on flexible substrate for long-term EEG monitoring *Sens. Actuators* B **244** 750–8
[21] Lin C-T, Liao L-D, Liu Y-H, Wang I-J, Lin B-S and Chang J-Y 2011 Novel dry polymer foam electrodes for long-term EEG measurement *IEEE Trans. Biomed. Eng.* **58** 1200–7
[22] Odinotski S *et al* 2022 A conductive hydrogel-based microneedle platform for real-time pH measurement in live animals *Small* **18** 2200201
[23] Lijnse T, Haider K and Dalton C 2022 High throughput fabrication of robust solid microneedles *Proc. SPIE* **11955** 119550E
[24] Oda Y, Kiso M, Kurosaka S, Okada A, Kitajima K and Hashimoto S 2008 Study of suitable palladium and gold thickness in ENEPIG deposits for lead free soldering and gold wire bonding (available at: www.semanticscholar.org/paper/Study-of-Suitable-Palladium-and-Gold-Thickness-in-Oda-Kiso/22153c7fcbf0ea37bc19f29fca52521df9731211) (Accessed 14 July 2022)
[25] Ranamukhaarachchi S A, Lehnert S, Ranamukhaarachchi S L, Sprenger L, Schneider T, Mansoor I, Rai K, Häfeli U O and Stoeber B 2016 A micromechanical comparison of human and porcine skin before and after preservation by freezing for medical device development *Sci. Rep.* **6** 32074
[26] Liu R X *et al* 2022 Mechanical evaluation of polymer microneedles for transdermal drug delivery: *in vitro* and *in vivo J. Ind. Eng. Chem. Res.* **114** 181–9
[27] Davis S P, Landis B J, Adams Z H, Allen M G and Prausnitz M R 2004 Insertion of microneedles into skin: measurement and prediction of insertion force and needle fracture force *J. Biomech.* **37** 1155–63
[28] Park J-H, Yoon Y-K, Choi S-O, Prausnitz M R and Allen M G 2007 Tapered conical polymer microneedles fabricated using an integrated lens technique for transdermal drug delivery *IEEE Trans. Biomed. Eng.* **54** 903–13
[29] Chen S, Li N and Chen J 2012 Finite element analysis of microneedle insertion into skin *Micro. Nano. Lett.* **7** 1206–9
[30] Loeters P *et al* 2004 Measuring the insertion of microfabricated microneedles into skin with a penetration sensor-web of science core collection *8th Int. Conf. on Miniaturized Systems for Chemistry and Life Sciences* (available at: www.webofscience.com/wos/woscc/full-record/WOS:000228997000167) (Accessed 7 July 2022)
[31] Roxhed N, Gasser T C, Griss P, Holzapfel G A and Stemme G 2007 Penetration-enhanced ultrasharp microneedles and prediction on skin interaction for efficient transdermal drug delivery *J. Microelectromech. Syst.* **16** 1429–40
[32] Ranamukhaarachchi S A *et al* 2016 Development and validation of an artificial mechanical skin model for the study of interactions between skin and microneedles *Macromol. Mater. Eng.* **301** 306–14
[33] Makvandi P *et al* 2021 Engineering microneedle patches for improved penetration: analysis, skin models and factors affecting needle insertion *Nano-Micro Lett.* **13** 93
[34] Zhang Y, Campbell S A and Karthikeyan S 2018 Finite element analysis of hollow out-of-plane HfO2 microneedles for transdermal drug delivery applications *Biomed. Microdevices* **20** 19
[35] Yan G, Warner K S, Zhang J, Sharma S and Gale B K 2010 Evaluation needle length and density of microneedle arrays in the pretreatment of skin for transdermal drug delivery *Int. J. Pharm.* **391** 7–12
[36] Coffey J W, van der Burg N M D, Rananakomol T, Ng H-I, Fernando G J P and Kendall M A F 2022 An ultrahigh-density microneedle array for skin vaccination: inducing epidermal cell death by increasing microneedle density enhances total IgG and IgG1 immune responses *Adv. NanoBiomed. Res.* **2** 2100151